22

Mass Transfer in the Electro-Dissolution of 90% Copper-10% Nickel Alloy in a Solution of Lithium Bromide

Martínez-Meza E., Uruchurtu Chavarín J. and Genescá Llongueras J.
Universidad Nacional Autónoma de México
México

1. Introduction

Copper is considered to be among the most important structural elements, just below iron and aluminum. Usually, the properties of this metal improve when combined with other elements (Kear et al., 2004b); the 90% Cu-10% Ni alloy has excellent physical, chemical and mechanical properties that allow it to adapt to different operating conditions (Kutz, 2002; Othmer, 2004). This metal is relatively inexpensive, as a structural element it is aesthetically attractive. It shows good thermal conductivity and a lower electrical resistivity than that observed both in the 70% Cu-30% Ni alloy and in steel; these characteristics make the 90% Cu-10% Ni alloy an efficient and competitive structural element in heat transfer processes (Copper-Nickel Alloys in Marine Environment).
In the last few decades, while trying to establish the dissolution mechanism in the presence of chlorides (Cl^-), this alloy has been the subject of numerous studies (Lee & Nobe, 1984; Crundwell, 1991; Milosev & Metikos, 1997; Kear et al., 2004b), usually at low concentrations and operating conditions close to those in the environment. However, its behavior in the presence of other agents such as bromides (Br^-), has received little attention (Itzhak & Greenberg, 1999; Muñoz-Portero et al., 2005), especially under operating conditions similar to those found in a heat pump that uses the H_2O-LiBr pair as a working fluid, which is very attractive because of its thermodynamic properties, however, it is very aggressive to the structural elements of the equipment (Muñoz-Portero et al., 2006).

1.2 Dissolution mechanism

The kinetics of dissolution of the 90% Cu-10% Ni alloy, in the presence of halides, shows marked similarities to the reaction mechanism of copper (Lee & Nobe, 1984; Crundwell, 1991; Kear et al., 2004a, 2004b).
In the Tafel region, in the vicinity of corrosion potential, three dissolution mechanisms have been proposed. Some researchers (Taylor 1971; Wagner et al., 1998; Kear et al., 2000, cited in Kear et al., 2004a) propose a two step mechanism; the first step consists in an electrochemical reaction, in which the cuprous ion (Cu^+) is produced due to the anodic dissolution of metallic copper (Cu). Then, in a chemical process, this species is combined with two chloride ions (Cl^-) to form the cuprous chloride complex ion ($CuCl_2^-$). However, due to thermodynamic matters, this is the least viable of the proposed mechanisms.

In studies carried out by (Walton & Brook, 1977, cited in Dhar et al., 1985) the same mechanism is proposed, concluding that the dissolution of the alloy takes place due to the degradation of a single component: copper. Meanwhile, (Beccaria & Crousier, 1989) speak of a simultaneous dissolution of both components, observing that copper is redeposited in the alloy.

The mechanism proposed by (Lee & Nobe, 1984; Crundwell, 1991; Deslouis et al., 1988a, 1988b) mentions that the alloy is dissolved through a process that takes place in two stages. It begins with the formation of cuprous chloride (CuCl) through an electrochemical reaction between Cu and the Cl^- ion. Later, in a chemical reaction between CuCl and the Cl^- ion, the $CuCl_2^-$ ion is formed. This reaction, according to (Kear et al., 2004b, 2007) is partly controlled by a mass transfer process.

Direct dissolution between Cu and two Cl^- ions through an electrochemical process to produce the $CuCl_2^-$ ion, has been adopted by other researchers (Kato et al., 1980a; Dhar et al., 1985; Muñoz-Portero et al., 2004; Kear et al., 2004b, 2007).

2. Results

2.1 Polarization curves

In the absence of oxygen, copper behaves according to the diagrams shown in (Figure 1(a)). In these circumstances, the metal reaches the E_{corr} at –437.4 $mV_{Ag/AgCl}$ at 25 °C; 28 mV, in more oxidizing conditions, it is reached at 55 °C.

Anodic polarization develops a slope of 75 mV/decade. This segment at 25 °C shows the turning point at -206.74 $mV_{Ag/AgCl}$ and generates a current of 3 mA/cm². As temperature increases, the active segment of the curve increases, developing at 55 °C a current of 9.5 mA/cm² to a potential of -219.1 $mV_{Ag/AgCl}$. The behavior of the curves after the inflection point is similar, however, the range widens, having the most unfavorable conditions at the upper temperature level with a current of 171.64 mA/cm² in the noblest part.

The range in the cathodic fraction opens in a significant way showing on the whole level, the establishment of limit currents. This current reaches a maximum value at the upper temperature level, developing at -870.18 $mV_{Ag/AgCl}$ a current of 0.195 mA/cm².

In the absence of oxygen, the 90% Cu-10% Ni alloy behaves as shown in the graphs (Figure 1(b)). In such circumstances, the development of a corrosive process controlled by activation can be observed across the anodic fraction only at 25°C. The curve in these circumstances reaches a slope of approximately 63 mV/decade. At -361 $mV_{Ag/AgCl}$ a slope change occurs, narrowing the activation process.

As temperature increases there is a turning point indicating an active-passive transition. At 35 °C, this change takes place at -347.51 $mV_{Ag/AgCl}$, generating a i_{crit} of 36 μA/cm²; then, the current drops to -298 $mV_{Ag/AgCl}$. When the slope increases again after this point, the curve displays a value of 72 mV/decade.

At the upper temperature level, the passive region is manifested in a wider range. "The passive primary potential" is established at -415.1 $mV_{Ag/AgCl}$, generating a i_{crit} of 34.18 μA/cm²; it is observed a reduction in the current until an inflexión point at –307.1 $mV_{Ag/AgCl}$. In such circumstances, a current of 8.5 μA/cm² is generated. From this point on, the current increases again. In this segment it develops a slope of approximately 50 mV/decade until a new inflexión point at –109.28 $mV_{Ag/AgCl,}$ from this point on the current is stabilized in a value of 107.34 mA/cm².

The system's E_{corr} is set in a 72 mV range, reaching at -458 $mV_{Ag/AgCl}$ the most oxidizing conditions at 35 °C. The cathodic part of the curve at the analyzed temperature level shows the development of limit currents, reaching its maximum value at 55 °C at -752.25 $mV_{Ag/AgCl}$.

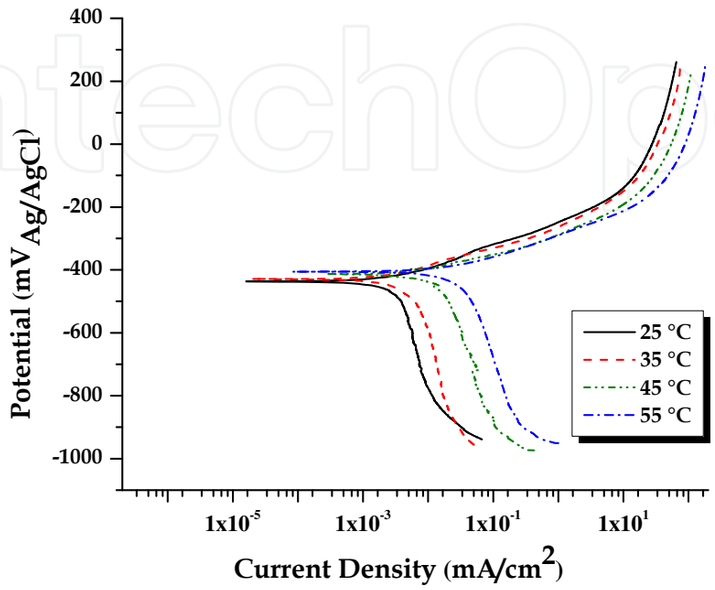

(a)

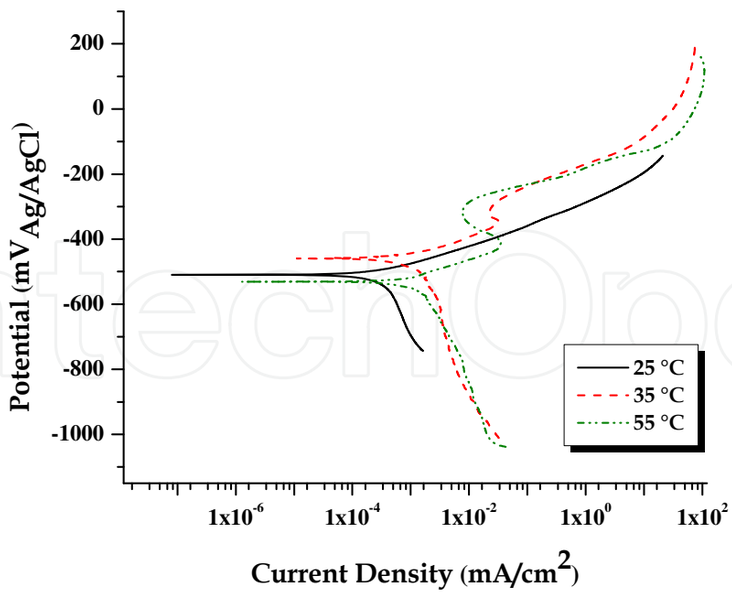

(b)

Fig. 1. Polarization diagrams the absence of oxygen and static conditions in 53% LiBr solution: (a) Copper, (b) 90% Cu-10% Ni

2.2 Impedance

Impedance spectroscopy is an appropriate technique to determine the electrical behavior of an electrochemical system, in which the system's general behavior is determined by a number of tightly coupled processes, each proceeding at a different speed (J. R. Macdonald). The diagrams in (Figure 2) show the behavior in the impedance spectrum of the 90% copper-10% nickel alloy in the 50% solution of LiBr, in the absence of oxygen, under static conditions at 25 °C.

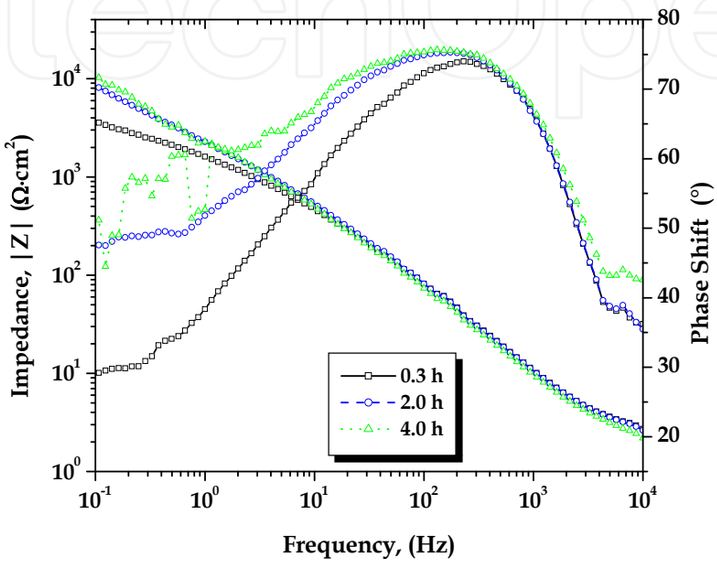

(a)

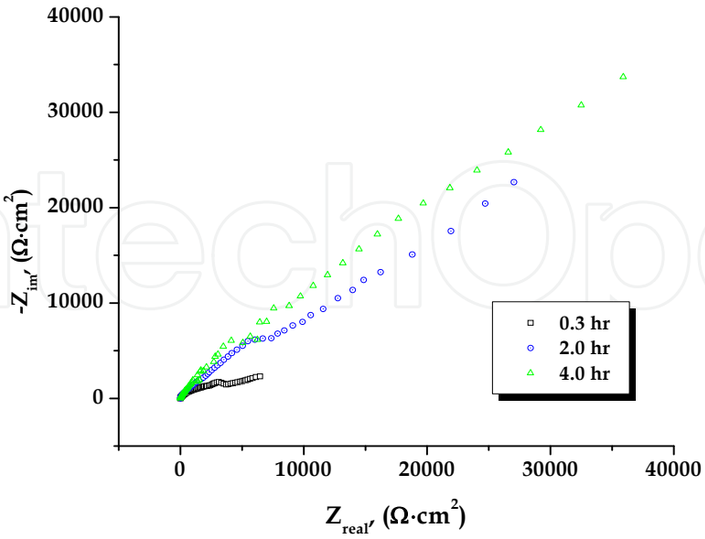

(b)

Fig. 2. Impedance spectrum of the 90% Copper-10% Ni-50% LiBr system, (a) Bode diagrams (b) diagrams in the complex plane

According to the Bode diagram, the system behaves similarly in the three periods of exposure up to a frequency of approximately 400 Hz. As this factor decreases, a mass transport phenomenon is manifested. This behavior is best seen in the complex plane, (Figure 2(b)). When the exposure period exceeds two hours, the development of a pure diffusion process is observed, which, due to its magnitude, dominates the metal dissolution process.

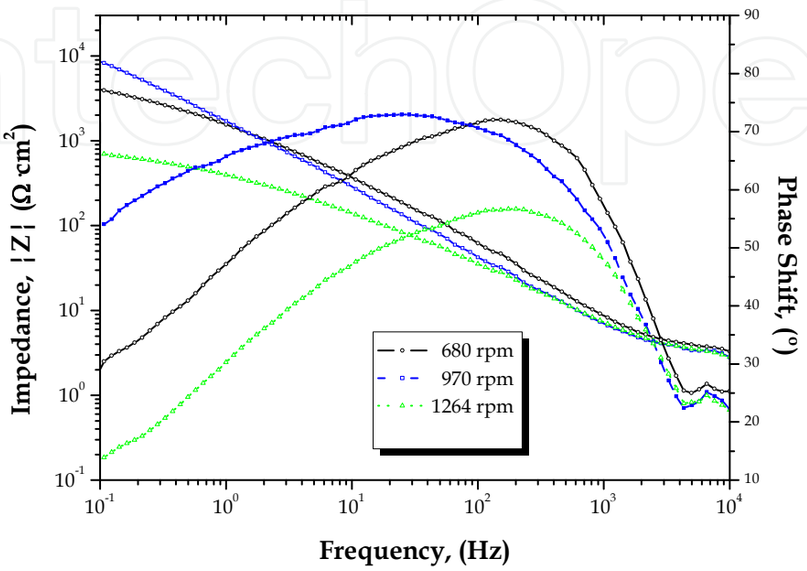

(a)

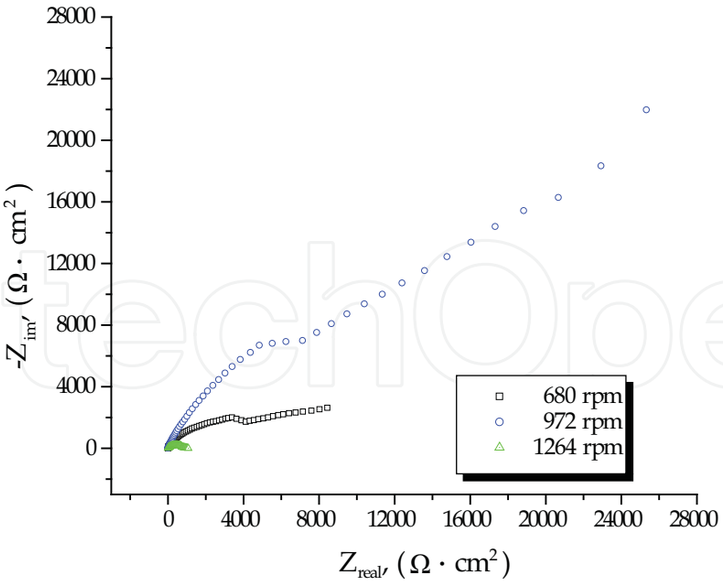

(b)

Fig. 3. Impedance spectrum for the 90% Copper-10% Nickel-50% LiBr system. Dynamic conditions at 25°C, at different rotation velocities, (a) Bode diagrams, (b) diagrams in the complex plane

The system behavior under dynamic conditions in the absence of oxygen is shown in the diagrams (Figure 3). In these circumstances the system behaves differently in the three rotation levels and only at 972 rpm, the development of a pure diffusion process can be observed, (Figure 3 (b)). As the rotation speed increases, the effect caused by this phenomenon decreases significantly. The behavior of the cell in the analyzed temperature range is synthesized in the values reported in Table 1. These parameters form the equivalent circuit (Figure 4), which acceptably describes the system behavior.

Temp. (°C)	Time (h)	rpm	E_{corr} ($mV_{Ag/AgCl}$)	R_Ω (Ω)	C_{dl} (μF/cm²)	R_{ct} (Ω·cm²)	Z_w (Ω·cm²)	Z_f (Ω·cm²)	|Z| (Ω·cm²)	θ (°)	$w_{(\theta=max)}$ (Hz)
25	0.3		-373.1	2.8	14.6	861	3,761	4,412	3,014	50	12.67
	2	0	-434.9	2.67	13.9	854	33,392	34,002	18,026	31.65	13.4
	4		-472.1	2.3	14.29	1,014	15,717	16,450	9,984	38.99	10.98
	-	680	-363.6	3.745	18.39	201	7,238	7,382	4,767	41	43
	-	972	-458.3	3.18	25.2	71	29,868	29,918	13,787	25.85	89
	-	1,264	-280.4	3.329	21.23	45	848.8	881	430	62.87	166.6
45	0.3		-387.3	3.2	15.8	255	5,993	6,176	4,090	42.86	39.5
	2	0	-420.9	3.35	19.4	230	21,059	21,222	11,626	32.61	35.6
	4		-435.7	3.37	20.7	234	22,825	22,991	12,167	31.16	32.9
	-	476	-402.9	3.15	18.2	147	17,305	17,409	10,060	34.89	59.5
	-	680	-355.8	2.86	23	198	1,225	1,372	957	49.48	35
	-	884	-344.5	2.91	21.4	170	972	1,099	772	50.24	43.8
60	0.3		-381.9	2	28.45	123.6	5,200	5,288	3,382	40.35	45.3
	2	0	-469.2	2.043	39.66	494.4	62,940	63,291	16,130	12.47	8.12
	4		-495.5	2.084	46.96	529.4	28,355	28,732	10,400	19.28	6.4
	-	380	-361	2.72	49.8	79	4,053	4,109	2,541	38.46	40.5
	-	543	-501.7	2.48	55.2	142	9,567	9,668	4,966	30.08	20.3
	-	706	-534.5	2.563	61.89	223.5	5,367	5,527	3,151	35.25	11.5

Table 1. Equivalent Circuit Parameters for System 90% Copper-10%Nickel-50% LiBr. Under Static and Dynamic Conditions

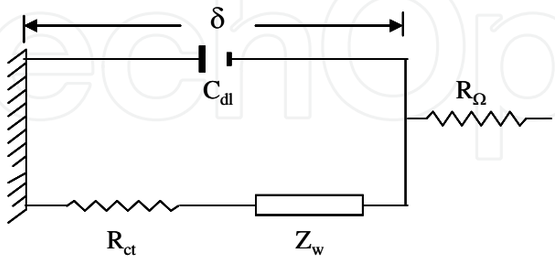

Fig. 4. Randles equivalent circuit, which describes the response of a system with a charge transfer process in one step coupled to a diffusion process at the interface

2.3 Electrochemical noise

The presence of noise processes in an electrochemical system is characterized by fluctuations in current and potential generated at random on the interface. This signal is a rich source of

information of a corrosive process; however, the signal as such masks phenomena occurring outside the charge transfer process (Hassibi et al., 2004).
The diagrams (Figure 5) show the behavior of the noise signal in current and potential in the time domain of copper-nickel alloy in the LiBr solution at different periods of exposure under static conditions at 25 °C.

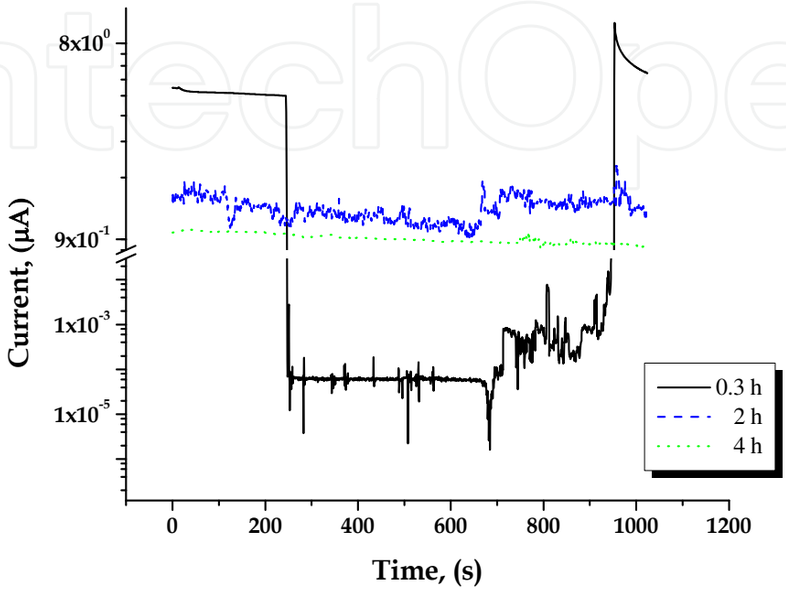

(a)

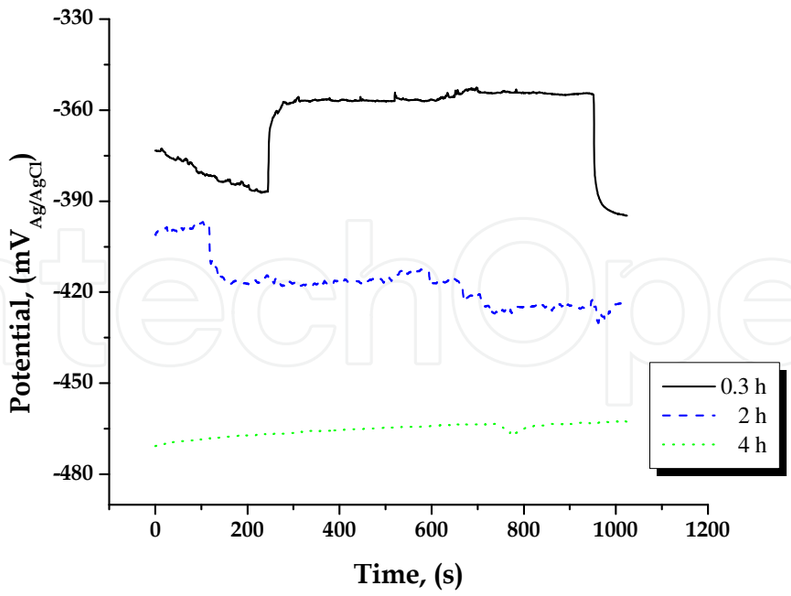

(b)

Fig. 5. Record in the time domain of noise signal in (a) current and (b) 90% Cu-10% Ni-50% LiBr system potential in static conditions at 25°C

The current and potential values in the time domain were obtained simultaneously. In the initial moments, in the test done at the 0.3 h, the current showed a very stable behavior. However, 250 s after the test started the current abruptly decreased about 5 logarithmic units until it reached a value of 5×10^{-5} μA. From that moment on, the development of transitional currents of a relative magnitude and frequency in the signal could be observed. However, it didn´t show a defined behavior pattern which suggests that this is the typical behavior of a pitting corrosion process. This phenomenon can be observed for a period of 700 s. Subsequently, the current increases again near the end of the registry, reaching a maximum value of 9.5 μA, and then decreases slightly. The current's behavior in the registry after two hours of exposure shows a more stable behavior over time, however, the development of a high frequency and low amplitude metastable process can also be observed, which reveals the origin of the signal, as this is caused by a more severe pitting corrosion process.

The current signal in the last period of exposure, after 4 hours, shows a fairly stable behavior over time, and due to the processes developed in the interface, the current generated in the system is lower compared to the previous test. Besides, judging by the shape of the graph, the development of a uniform corrosion process can be predicted.

As for the potential, the signal at 0.3 h of exposure showed the following behavior. In the first 250 s the potential moves in an active direction approximately 14 mV, and then suddenly shifts towards a noble direction 30 mV, remaining virtually unchanged during the next 700 s. Later, near the end of the test, the signal registered again a major shift toward an active direction. After two hours of exposure, the signal record is irregular, suggesting that its origin is a random pitting corrosion process; the signal is developed in a more active region, also showing a very small dc trend. As for the last test, in these conditions the signal seems to be fairly stable in all directions moving further into an active region.

In flow conditions, the records for both current and potential noise generated by the system at 45°C in the absence of oxygen are shown in the diagrams (Figure 6). In contrast to the behavior shown by the system at a lower temperature level, the current generated in the cell at 45°C decreases significantly as the electrode velocity increases. At a velocity of 680 and 884 rpm the current signal reaches during the initial moments a stationary state, maintaining this condition during the development of the test. Under these conditions the signal gives the impression of having been filtered, however, it is the original signal.

The behavior of the potential noise signal can be considered normal because as the electrode velocity increases, the signal shifts to a nobler region. Despite the fact that the potential noise signal at 884 rpm seems a bit irregular during its registry, it shows a trend of only 3 mV. At 476 rpm the trend in the signal was 35 mV, and during the record of this period, the signal did not reach the stationary state.

Table 2 shows the resistance value for each experimental condition determined by different electrochemical techniques used for that purpose. Also, a comparison of the values obtained by filtering the signal is shown in it. The difference is significant and is almost constant throughout the experimental range. This was the main reason for deciding to work with the original signal from the current and potential records over time.

1. Resistance in noise measured before and after removing the dc component of the signal,
2. Resistance in noise measured after removing the dc component with the average removal method, MAR (Tan et al., 1996).

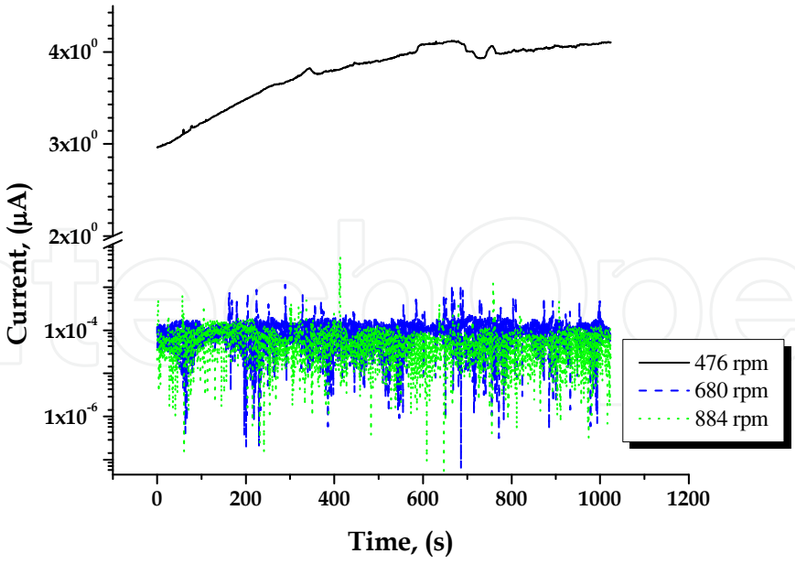

(a)

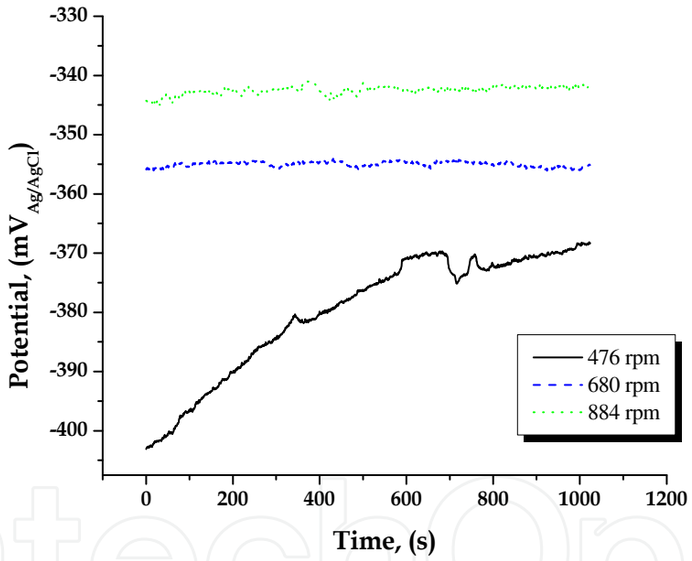

(b)

Fig. 6. Record in the time domain of noise signal (a) current and (b) potential, 90% Cu-10% Ni-50% LiBr system potential under flow conditions at 45°C

For this reason it is assumed that the signal is due solely to charge transfer processes. When the velocity is increased, due to the generation of transitory currents of high frequency and relative amplitude, the development of a pitting corrosion process could be considered. However, this phenomenon is not reflected in the potential noise signal, either because there is no such process or because the current generated in these conditions is very small. Statistically, the average current value at 884 rpm is 4.47×10^{-8} μA. At 476 rpm the oscillatory phenomenon in the current is not seen, on the contrary, a fairly stable signal is shown, with a tendency of just 1 μA.

Temperature (°C)	Time (h)	Velocity (rpm)	$Rn_{(1)}$ ($\Omega \cdot cm^2$)	LPR ($\Omega \cdot cm^2$)	Z_f ($\Omega \cdot cm^2$)	$Rn_{(2)}$ ($\Omega \cdot cm^2$)
25	0.3	-	4,283	7,366	4,412	1,853
	2	-	37,244	24,977	34,002	4,759
	4	-	32,637	113,789	16,450	5,068
	-	680	13,905	9,375	7,382	90,859
	-	972	20,527	18,092	29,918	40,556
	-	1,264	6,613	649	881	11,315
45	0.3	-	3,273	7,704	6,176	1,412
	2	-	25,205	18,413	21,222	1,553
	4	-	28,247	30,306	22,991	1,549
	-	476	24,527	17,974	17,409	26,683
	-	680	2,699,167	3,377	1,372	491,550
	-	884	3,219,963	2,383	1,099	303,667
60	0.3	-	8,810	8,352	5,288	1,063
	2	-	50,941	40,317	63,291	1,489
	4	-	146,872	61,506	28,732	35,449
	-	380	5,408	1,800	4,109	803
	-	543	20,942	14,130	9,668	3,905
	-	706	22,938	12,565	5,527	6,650

Table 2. Resistance determined using different electrochemical techniques Static and dynamic conditions for the 90% Cu-10% Ni-50% Lithium Bromide System

The corrosion rate i_{corr} of the system is obtained using the Tafel slopes and polarization resistance Rp, along with the Stern-Geary relationship, equation 1, (Stern & Geary, 1957; Mansfeld F., 1973a, 1973b)

$$i_{corr} = \frac{\beta_a \beta_c}{2.3(\beta_a + \beta_c)} \frac{1}{R_p} = \frac{B}{R_p} \tag{1}$$

Where β_a and β_c are the anodic and cathodic Tafel slopes, respectively.

Temp. (°C)	Time (h)	Velocity (rpm)	E_{corr} ($mV_{Ag/AgCl}$)	R_n ($\Omega \cdot cm^2$)	LPR ($\Omega \cdot cm^2$)	Z_f ($\Omega \cdot cm^2$)	i_{corr} (B=0.026)		
							($\mu A/cm^2$)$_{(Rn)}$	($\mu A/cm^2$)$_{(LPR)}$	($\mu A/cm^2$)$_{(Zf)}$
25	0.3	-	-373.1	4,283	7,366	4,412	6.07	3.528	5.893
	2	-	-434.9	37,244	24,977	34,002	0.698	1.04	0.765
	4	-	-472.1	32,637	113,789	16,450	0.796	0.228	1.58
	-	680	-363.6	13,905	9,375	7,382	1.869	2.77	3.522
	-	972	-458.3	20,527	18,092	29,918	1.266	1.44	0.869
	-	1,264	-280.4	6,613	649	881	3.931	40	29.5

Table 3. Corrosion Rate in Static and Dynamic Conditions of the 90% Cu -10% Ni Alloy in a 50% Lithium Bromide solution at 25°C

2.4 Kinetic parameters

According to the values reported in Table 1 and the proposed equivalent circuit (Figure 4), the dissolution of the alloy is under mixed kinetic control, by activation and diffusion. However, the mass transport resistance under all experimental conditions is higher than that observed for charge transfer. On the other hand, as both elements are in series, the one representing the mass transport process shows more resistance to current flow. Therefore, the diffusion phenomenon should be the process that controls the dissolution of the alloy.

For the dissolution process to be maintained, the reacting species must match on the interface in an electrochemical process. Transport to the electrode surface is given by a combination of two phenomena. First, by a convective process from the bulk of the solution to the outside of the film. Subsequently, the reagent must diffuse through this layer to reach the electrode surface (Brossard & Raynaud, 1985).

According to the values in Table 1, mass transfer controls the kinetics of the system; however, it didn´t always follow the Levich relation. The oxygen diffusion coefficient was determined for those conditions that apply to this relation according to the following equation (Bard & Faulkner, 1980; Barsoukov & Macdonald, 2005).

$$D_{o_2} = \left[\frac{R\,T}{\sigma\, n^2\, F^2\, \sqrt{2}\, C_{o_2}} \right]^2 \tag{2}$$

Where:

σ, Warburg coefficient, Ω $s^{1/2}$; R, gas constant, 8.314 J mol^{-1} K^{-1}; F, Faraday constant, 96,485.309 C mol^{-1}; T, temperature, K; C_{O_2}, Oxygen concentration, mol cm^{-3}; D_{O_2}, Diffusion coefficient, cm^2 s^{-1}; n, number of electrons transferred in reaction

The film thickness δ under static conditions was determined according to the following equation (Bard & Faulkner, 1980).

$$\delta = \frac{n\, F\, D_{o_2}\, C^*_{o_2}}{i_L} \tag{3}$$

Where:

i_L, cathodic limit current density, A cm^{-2}; $C^*_{O_2}$, Oxygen concentration within the solution, mol cm^{-3}

Under flow conditions, the thickness was determined by the following equation

$$\delta = 1.61\, D_{o_2}^{1/3}\, w^{-1/2}\, \gamma^{1/6} \tag{4}$$

Where:

w, angular velocity, radians s^{-1}; γ, kinematic viscosity, cm^2 s^{-1}

The exchange current density i_o and the rate constant k_o were determined according to the following equations

$$i_o = \frac{RT}{nFR_{ct}} \tag{5}$$

Where:

R_{ct}, Resistance to charge transfer, Ω·cm^2

$$k_o = \frac{RT}{n^2 F^2 R_{ct} C_{CuBr}} \quad (6)$$

Where:
C_{CuBr} Solution concentration, mol cm^{-3}
The results in Table 4 show the diffusion coefficient and the thickness of the film only on those system conditions where the Levich relation was followed.

Temperature (°C)	Time (h)	Velocity (rpm)	E_{corr} ($mV_{Ag/AgCl}$)	$i_0 \times 10^5$ (A/cm^2)	$D_{O_2} \times 10^5$ (cm^2/s)	$k_0 \times 10^8$ (cm/s)	δ (μm)
25	0.3	-	-373.1	2.98	-	3.5	
	2	-	-434.9	1.2	0.149	0.5	1.14
	4	-	-472.1	1	0.123	0.4	1.89
	-	680	-363.6	12.79	-	15	
	-	972	-458.3	14.5	0.218	6.8	10.9
	-	1,264	-280.4	57.17	-	67.3	
45	0.3	-	-387.3	10.75	-	12.6	
	2	-	-420.9	4.8	1.53	2.2	3.44
	4	-	-435.7	4.7	0.675	2.2	2.33
	-	476	-402.9	18.65	65.8	21.9	98.1
	-	680	-355.8	13.84	-	16.3	
	-	884	-344.5	16.13	-	18.9	
60	0.3	-	-381.9	23.22	611.2	27.3	1,284.20
	2	-	-469.2	2.32	-	1	
	4	-	-495.5	2.17	-	1	
	-	380	-361	36.34	-	42.7	
	-	543	-501.7	8.1	1.83	3.8	26.9
	-	706	-534.5	5.14	-	2.4	

Table 4. Kinetic Parameters for System 90% Copper-10% Níkel-50% Lithium Bromide Under Static and Dynamic Conditions

3. Discussion

According to the Pourbaix diagram for the Cu-Br – H_2O system at 25°C (Muñoz-Portero et al., 2004), the only products of metal corrosion in the Tafel region and acidic conditions are: cuprous bromide, CuBr, and the complex ion $CuBr_2^-$. These species are formed according to the following reactions:

$$Cu + Br^- \rightarrow CuBr + 1\,e^- \quad (7)$$

With an equilibrium potential at 25°C defined by the following equation

$$E_{(Cu/CuBr)} = 0.031 + 0.0591 \log\left[\frac{1}{Br^-}\right]; V_{(SHE)} \quad (8)$$

The complex ion formation requires the participation of two units of bromide ion producing tha same amount of charge

$$Cu + 2\,Br^- \rightarrow CuBr_2^- + 1\,e^- \tag{9}$$

With an equilibrium potential at 25ºC defined by the following equation

$$E_{\left(Cu/CuBr_2^-\right)} = 0.195 + 0.0591 \log\left[\frac{\left(CuBr_2^-\right)}{\left(Br^-\right)^2}\right]; V_{(SHE)} \tag{10}$$

Anodic polarization of the cell in the Tafel region develops slopes in a range of 60 to 75 mV/decade, Figure 1. (Lee & Nobe, 1984) determine the slope in a chloride solution at approximately 60 mV/decade. This fact implies that the dissolution of the electrode is accomplished by activation. However, these researchers argue that the electro-dissolution of metal is controlled by a mass transport process. The value of this parameter (Pérez-Herranz et al., 2001) is in a range of 70 to 80 mV /decade, for a velocity range of 265 < Re <3,120. This range is close to slopes of 60 mV/decade, typical of a metal dissolution process controlled by diffusion of products from the metal surface to the bulk of the solution. The active dissolution region observed at potentials nobler than E_{corr}, the author goes on, is consistent with the formation and dissemination of the complex ion, and when this phenomenon increases, it alters the anodic Tafel slopes. (Kear et al., 2004b) provides a summary of several research papers on chlorides determining the anodic slope at different operating conditions.
The electrochemical reaction rate is limited by environmental factors, both physical and chemical, so that the reaction is polarized or delayed due to these factors. Activation polarization refers to an electrochemical process controlled by the slowest step in a reaction sequence on the interface. Polarization can be defined as the displacement of the electrode potential due to a net current flow and its magnitude is overpotential η, which is a polarization measure with respect to the equilibrium potential of the electrode (Fontana & Greene, 1978)
The relationship between reaction rate and η due to activation polarization is

$$\eta_a = \pm \beta_a \log \frac{i}{i_o} \tag{11}$$

Above is the Tafel equation, where β is frecuently known as the Tafel slope or constant and I_o has been defined before

$$\beta_a = \frac{2.303\,RT}{\alpha nF} \tag{12}$$

α is the transfer coefficient, the constants R, T, F and n were defined before.
The Tafel law (Bockris et al., 2000) shows the exponential relationship between reaction rate and the η. This approach can be seen clearly in the dissolution of copper and in the 90/10 alloy, Fig. 1. (Lee & Nobe, 1984, Fig 2, 4-5) claim that the anodic behavior in this region is an "apparent" Tafel behavior, since it doesn´t represent an activation controlled process. This idea is shared by other researchers, however, (Kato & Pickering, 1984; Pérez-Herranz et al., 2001) despite stating that for a slope of 60 mV/decade the anodic process is controlled by diffusion, determine the i_{corr} by the Tafel extrapolation method (Fontana & Greene, 1978;

Flitt & Schweinsberg, 2005), which is well known and often poorly implemented. Researchers often forget that the metal needs to corrode evenly, and in the corrosion potential the anodic and/or cathodic reactions must be under complete control by activation. Furthermore, in order to estimate the i_{corr} correctly, the linear portion identified in the curves should extend at least a decade on the current's logarithmic scale. The i_{corr} is calculated by (Deslouis et al., 1988a) assuming a pure activation mechanism for both fractions, which is contrary to their approach.

As the potential shifts in noble direction the curve develops a gradual change of slope. At about -200 $mV_{Ag/AgCl}$, this change takes place virtually under the same conditions (Cooper & Bartlett, 1958; Brossard, 1984a, 1984b; Wood et al., 1990; Muñoz-Portero et al., 2005) thus indicating that the dissolution mechanism is changing. The end of the apparent Tafel region is associated with the formation of CuBr (Brossard, 1984b; Valero-Gómez et al., 2006). A similar pattern was seen in the work of (Pérez-Herranz et al., 2001) at a Re = 263. This behavior was attributed by (Aben & Tromans, 1995 cited in Pérez-Herranz et al., 2001) to the CuBr formation, and the stationary current observed at nobler potentials was attributed to the presence of a CuBr passive film. This behavior was also observed (Lal & Thirsk, 1953, quoted in Kear et al., 2004a; Deslouis et al., 1988a) in a solution of Cl-, however, when $[Cl^-] \geq 2$ mol/l , the development of critical current density is not observed due to a faster dissolution of the CuCl layer, which is why they take on a film-free surface.

However, Deslouis attributes this behavior to the fact that the reaction equilibrium, equation 13, changes, favoring the formation of the complex ion.

The relationship between species CuBr, Br^- and $CuBr_2^-$ helps define some significant differences in the approach given to this system's dissolution process. The equilibrium between these species is defined through the following reaction

$$CuBr + Br^- = CuBr_2^- \tag{13}$$

At 25°C equilibrium is defined according to the following equation

$$\log\left(CuBr_2^-\right) = \log\left(Br^-\right) - 2.778 \tag{14}$$

In the active state, reactions, equations 7 and 9, properly describe the behavior of the system, since both proceed on the same energy level, having the same equilibrium potential, which suggests that they are thermodynamically equivalent. This is contrary to the dissolution mechanism proposed by (Kato et al., 1980a; Brossard, 1984a, 1984b; Dhar et al., 1985; Muñoz-Portero et al., 2004; Kear et al., 2004b, 2007).

Table 5 shows the equilibrium potential for equation 8 in function of the Br^- ion activity and temperature (Appendixes A-C). Values in parentheses show the equilibrium potential for equation 10.

According to the information in Table 5, the $E_{Cu/CuBr}$, consistently moves an average of 98 mV in an active direction due to the $[Br^-]$ and 17 mV due to the effect of temperature. The analysis would seem trivial and out of context if not for the fact that this behavior and the linear relation of the potential and the logarithm of current density, E vs log i, equation 11, with a slope close to 60 mV/decade were taken as a basis for claiming that the dissolution rate of copper in a solution of Cl^- in a potential close to E_{corr}, goes on under the influence of a combined process of diffusion and activation. The first to demonstrate such behavior were (Lal & Thirst, 1953, quoted in Kear et al., 2004a, Fig. 4), in these circumstances (Crundwell, 1991) falls into contradiction.

Temperature	$E_{CuBr/Cu}$ ($mV_{Ag/AgCl}$)			
(°C)	**40%**	**50%**	**53%**	**60%**
25	-355.6	-400.1	-415.6	-453.9
	(-355.7)	*(-400.9)*	*(-415.9)*	*(-454.22)*
35	-358.8		-418.8	-457.2
45	-363.1	-408.2	-423.1	-461.4
55	-368.7		-428.4	-466.5
60	-373.1	-418	-432.7	-470.7

Table 5. Copper-X% Lithium Bromide System, Equilibrium Potentials

If the system proceeds according to equation 7, as the potential moves in a positive direction to the inflection point, the CuBr formation will increase significantly. The CuCl formation on the electrode surface is observed at η = 16 mV and the covered area increases as the potential becomes nobler (Brossard, 1984a, 1984b). On the other hand (Bjorndahl & Nobe, 1984 and Dhar et al., 1985, cited in Deslouis et al., 1988a), they take on an oxide-free surface.
In the electrochemical process, the atoms on the surface react with the Br^- ion of the solution by generating a charge unit and the CuBr compound, which is poorly soluble, $k_{ps} = 6.27 \times 10^{-9}$, (Weast, 1984), which is why it precipitates and adheres to the electrode surface. In a second step, through a chemical process, the substance continues to react with the Br^- ion in the solution, dissolving at a constant rate, equation 13, even after polarization is interrupted (Crundwell, 1991). The dissolution rate of the precipitate is constant until dissolution is complete (Brossard & Raynaud, 1985), finally producing the complex species, which is soluble and diffuses into the bulk of the solution. (Lal & Thirsk, 1953 cited in Kear et al., 2004a) found that the formation of $CuCl_2^-$ is consistent with increases in the potential for a given $[Cl^-]$.
The anodic behavior of the system can be described in a fairly acceptable way with the combination of equations 7 and 13. Thus, the dissolution mechanism takes place due to a simultaneous process in two stages. The mathematical model that best describes the dissolution of this metal corresponds to this mechanism (Deslouis et al., 1988a). A common mechanism may explain the process in acidic and neutral environments (Deslouis et al., 1993), however, this assertion is not possible due to thermodynamic matters.
Typically, the corrosion potential of the cell was established in the stability region of water. In a nobler region compared to the hydrogen electrode, but well below the oxygen electrode potential, which ultimately controls the cathodic portion of the system. Under flow conditions, this behavior can be seen more clearly as shown in (Pérez-Herranz et al., 2001, Fig. 2). By increasing the flow rate, the current value in the cathodic fraction increases significantly; however, the response of the anodic branch is more discreet to these changes.
A similar behavior suggests that the partial anodic fraction is more affected than the cathodic fraction by mass transfer (Deslouis et al., 1988a). According to Pérez-Herranz, the limit current observed in the cathodic fraction is attributed to hydrogen evolution. During the dissolution process, protons (H^+) diffuse to the metal surface, so if the dissolution rate is controlled by this current, the diffusion of protons could be seen as the step that determines the metal's rate of dissolution. The displacement of E_{corr} in a noble direction as velocity increases could be attributed to the control of the cathodic reaction due to the detachment of clusters of hydrogen molecules from the metal surface, which improves as velocity increases

(Brown et al., 1992, cited in Pérez-Herranz et al., 2001; Montañés et al., 2006). According to (Muñoz-Portero et al., 2005), pH causes the current to increase and the potential to shift to a nobler zone, restricting the passive zone. The electro-dissolution of copper is essentially independent from pH (Brossard, 1984a).

3.1 90% Copper-10% Nickel-X% Lithium Bromide System

As an average, in the range 40% ≤ [Br-] ≤ 60% and 25°C ≤ T ≤ 60°C, the alloy E_{corr} moves, compared to the copper E_{corr}, 57 mV in a negative direction. This is due only the presence of nickel and is crucial to establish a significant difference in the behavior of both materials. (Kato et al., 1980a) report that the alloy E_{corr} is 10 mV nobler.

The nickel in the LiBr solution, under the conditions of this investigation, dissolves according to the Ni-H_2O-Br system (Muñoz-Portero et al., 2007) as follows:

$$NiH_{0.5} + 2\,Br^- \rightarrow NiBr_{2(s)} + 0.5\,H^+ + 2.5\,e^- \tag{15}$$

With an equilibrium potential at 25°C according to the following equation

$$E = -0.04543 + 0.02365 \log\left[\frac{1}{(Br^-)^2}\right] - 0.011827\ pH \tag{16}$$

Generally, under the conditions in which the alloy E_{corr} is established, copper is found in a condition of immunity (Tables 1 and 5).

For example, in the 40% LiBr solution at 25°C, the alloy E_{corr} -393.22 $mV_{Ag/AgCl}$ is found 37.62 mV in a more active region compared to the copper equilibrium potential $E_{CuBr/Cu}$, -355.6 $mV_{Ag/AgCl,}$ and is polarized compared to the nickel equilibrium potential $E_{NiH_{0.5}/NiBr_{2(s)}}$, with an η_a of 78.2 mV, (Martínez-Meza E, 2011).

(Brossard, 1984a) observed a surface free of corrosion products at more active potentials than $E_{Cu/CuCl}$.

Under these conditions, in the E_{corr} vicinity, the anodic fraction of the system is due to nickel dissolution, according to the above reaction, equation 15. This could be the reason why (Lee & Nobe, 1984) observed a selective nickel electro-dissolution.

The composition of the reaction products depends heavily on the potential. At more active potentials nickel dissolution is favored; therefore the reaction products contain higher nickel concentrations than the alloy (Milosev & Metikos, 1997). (Cahan & Haynes, 1969, cited in Lee & Nobe, 1984) conclude that the overall reaction is controlled by nickel dissolution. However, as explained below this behavior is not possible in the alloy, otherwise it wouldn´t passivate. (Kato & Pickering, 1984) claim that the selective dissolution of copper doesn't take place when significant concentrations of nickel are found in the layers of corrosion products. (Dhar et al., 1985) state that the role of nickel in the corrosion process is not evident. In this sense (Crundwell, 1991) obtained contradictory results.

When the system is anodically polarized due to the kinetics of copper in the 53% solution and to a temperature of 25°C with the presence of oxygen, for example, $i_o = 7.3 \times 10^{-6}$ A cm^{-2}, this metal dissolves more rapidly than nickel, $i_o = 0.523 \times 10^{-6}$ A cm^{-2}. Thus, this element has a main role in the dissolution of the alloy (Martinez-Meza E, 2011). As the potential increases, the selective electro-dissolution of nickel gradually decreases and the electro-dissolution of copper increases (Lee & Nobe, 1984). For this reason the polarization diagrams of both copper and the 90/10 alloy are similar. The polarization and E_{corr}

characteristics of the 90/10 alloy show a marked similarity to those of copper (Crundwell, 1991; Kear et al., 2004b). (Kear 2001 cited in Kear et al., 2004b) found in dynamic conditions 200 < rpm < 9.500 that the morphology of the anodic fraction of the alloy was similar to that determined independently for copper. On the other hand (Milosev & Metikos, 1997) support the similarity of the two systems using cyclic voltammetry. However, an E_{corr} in more active areas and a smaller i_{corr} in the 90/10 alloy show significant differences between these materials. When the CuNi-90/10 polarization exceeds copper $E_{Cu/CuBr}$, the alloy corrodes due to the dissolution of both elements according to equation 7, 13 and 15. The alloy in the 53% solution at 35 and 55°C (Figure 1 (b)) shows an active-passive behavior. This behavior is observed in the work of (Kato et al., 1980a; Lee & Nobe, 1984) and (Walton & Brook, 1977 cited in Lee & Nobe, 1984), unfortunately, this behavior was not understood.

According to Lee, the dissolution of the CuCl film is the dominant process in this region, and is under mass transfer control, the diffusion of the complex ion to the bulk of the solution.

This behavior according to the Pourbaix diagrams for the Cu-H_2O-Br and Ni-H_2O-Br systems, (Muñoz-Portero et al., 2004, 2007) is not explained by the presence of an oxidized compound which could passivate the electrode. This behavior is due to a very aggressive copper dissolution, causing the electrode surface to be enriched in nickel.

By increasing the concentration of nickel, the 90/10 ratio is modified in such a way that the alloy passivates due to the characteristics of nickel. Under these conditions, it is likely that a Cu/Ni relation between 1.9 and 2.2 will be established. When the relation is established on the upper level the probable concentration of nickel on the electrode surface is 31.25% by weight. There is a critical composition of nickel in the alloy (Mansfeld & Uhlig, 1970) over which the polarization curves exhibit a passive current density similar to that shown by nickel, and under which passive current density disappears, causing the alloy to behave like copper.

According to the theory of electronic configuration, metals with orbital vacancies in "d", also known as transition metals are known to favor the chemisorption of oxygen. Therefore, passivity in the alloy is only observed when the vacancies in these orbitals are present. When such vacancies have been occupied by electrons of the alloy components, the necessary chemisorption of oxygen required to cause passivation does not occur.

This behavior is typical of an adsorption process as the one observed in stainless steel. For this reason it is not uncommon to assume that under these circumstances, a passivation process occurs, similar to that observed in these materials.

The standard Flade potential E_F^0 for nickel is 0.2 V_{SHE} (Uhlig & Revie, 1985); therefore, the Flade potential, passivation potential, for the alloy in the 53% LiBr solution is given in correspondence to the equation.

$$E_F = 0.2 - 0.059\,pH;\ V_{(SHE)} \tag{17}$$

Under these conditions the system presents a passivation potential of -301.85 $mV_{Ag/AgCl}$. In the charts this potential is observed at -298 and -307.1 $mV_{Ag/AgCl}$ for the system at 35 and 55°C, (Figure 1(b)).

For this reason, it can be said that under these conditions the alloy passivates due to an oxygen chemisorption process, and not because of the formation of a CuBr film, which is why the complex species does not spread in this region. However, due to the instability of the film and the Br^- ion concentration, the film dissolves quickly.

The 90% Cu-10% Ni-50% LiBr system during the first period, 0.3 h, invariably reaching the E_{corr}, Table 1, in nobler conditions respect to $E_{Cu/CuBr}$, Table 5. In the impedance spectrum at 25°C, a resistance of 3.01 kΩ·cm² is developed. As the exposure time goes by, the value of this parameter increases, reaching its maximum value after two hours, at 25 and 60°C. The cell at 45°C, in the last two periods, develops a similar value close to 12 kΩ·cm².

The cell reaches the E_{corr} in nobler conditions due to increased oxygen presence in the solution. In these circumstances a segment of the cathodic fraction, close to E_{corr} develops a Tafelian behavior (Figure 7) before reaching a limit current status, and for this reason, the diffusion phenomenon shows less presence.

At 60°C the contribution of this factor is 5.2 kΩ·cm². As time of exposure goes by, E_{corr} is reached at more reducing conditions. Apparently this behavior is generated by the system itself, either because of a lower oxygen concentration in the interface due to the same process of dissolution, or by an enrichment of nickel on the electrode surface due to copper dissolution.

Under these conditions, oxygen diffusion turns relevant, becoming the step that controls the dissolution rate. At 25°C, the i_L goes from 13.58 μA/cm² in the first period to 1.9 μA/cm² after 4 hours. At 60ºC, i_L goes from 5.74 μA/cm² at 0.3 h to 2.6 μA/cm² in the last period (Figure 7(a)). After two hours of exposure, the system at 60°C develops the highest mass transport resistance, 62.9 kΩ·cm², Table 1.

The film causes a substantial decrease in the oxygen reduction rate. This reaction near E_{corr} potentials is more affected by corrosion products than the anodic reaction. In the Tafel region, the formation of the layer significantly affects the cathodic fraction, only mildly affecting the anodic fraction, which indicates a cathodically controlled corrosive process (Hack & Pickering, 1991). Thus, oxygen reduction can be regarded as the most important reaction to determinate the general corrosion rate in the presence of a protective film (Kato et al., 1980b).

(Kear et al., 2004a) present a list of equations developed by different researchers, which describe copper dissolution in a chloride solution in the apparent Tafel región. Almost all of them regard the process as reversible and dependent on a combined charge transfer and mass transport process. The diffusion of $CuCl_2^-$ complex ion from the electrode surface to the bulk of the solution, takes control in mass transport.

As mentioned before, during the first period of exposure 0.3 h, the cell E_{corr} invariably moves towards a noble direction respect to $E_{Cu/CuBr}$, reflecting an anodic polarization at 25°C of 27.58 mV. This behavior indicates that the system is not in equilibrium. (Deslouis et al., 1988b, 1993) consider the electro-dissolution to be in pseudo-equilibrium, in such a way that can not be considered reversible. The establishment of a reversible state applies for a half-cell reaction, but is not appropriate to describe a corrosive system.

In dynamic conditions, especially at 45°C, the effect of velocity on the system is clearly shown, because as it increases the E_{corr} moves towards a noble direction and the i_L is increased (Figure 7(b)). This effect of velocity is typical of a diffusion-controlled cathodic process (Fontana & Greene, 1978).

(Kear et al., 2004a) mention that in the three copper dissolution mechanisms in a chloride solution proposed to date, it is generally assumed that the anodic reactions are reversible, and it is universally accepted that they are all under a mixed kinetic control near the corrosion potential.

According to Figure 5, in static conditions a few seconds are needed to appreciate the formation of corrosion products on metal surface. 40 seconds of oxidation are sufficient to form a layer of corrosion products that fully cover the electrode (Brossard & Raynaud, 1985).

In this regard, the system's response depends on the operating conditions thereof, as the diffusive barrier morphology varies according to temperature as shown the images (Figure 8) (Brossard & Raynaud, 1985).

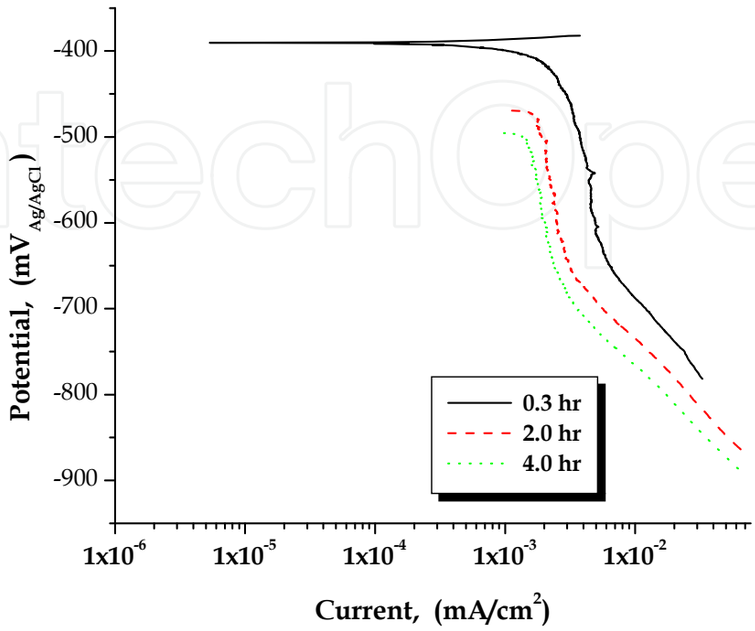

(a)

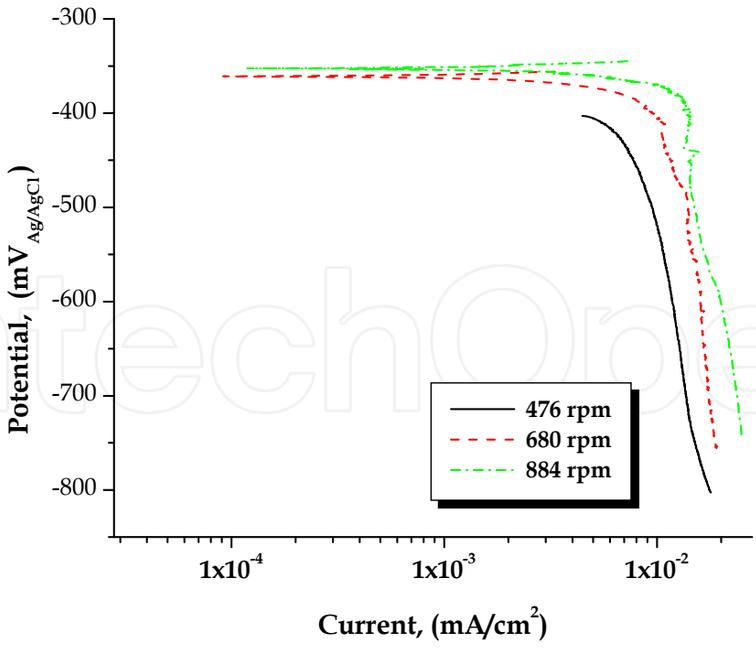

(b)

Fig. 7. Cathodic polarization of the 90 % Cu-10% Ni-50% LiBr system, (a) in static conditions at 60°C (b) in dynamic conditions at 45°C

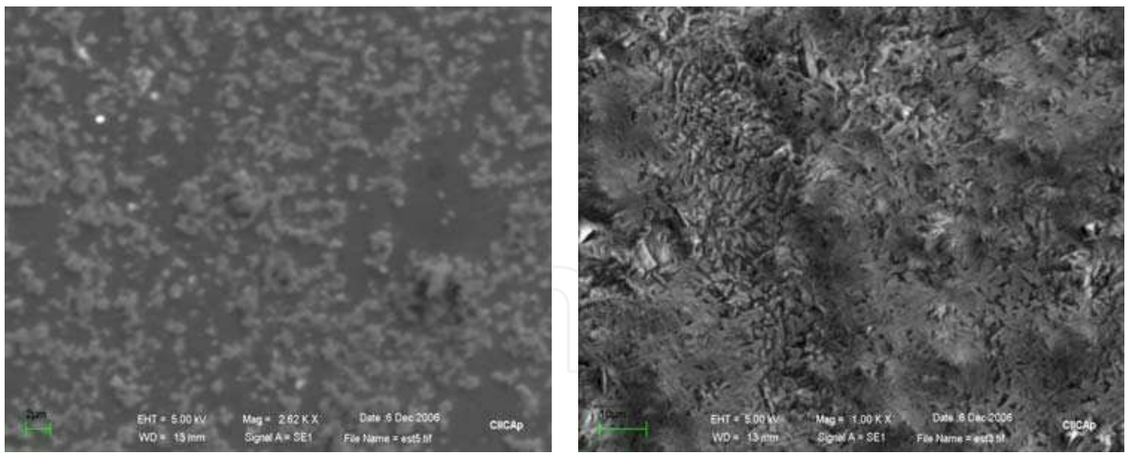

(a) (b)

Fig. 8. Images taken with scanning electronic microscope, showing the electrode surface after the tests made in static conditions in the absence of oxygen (a) 25°C and (b) 60°C

The morphology of the film formed at 25°C is characteristic of a uniform corrosion process, noting in the first period of exposure an important amount of particles adhered to the electrode surface. The film formed at 60°C (Figure 8(b)) shows a rather compact morphology, very different from the response of the system at 25°C.

This difference can be seen in the response of the system, Tables 1 and 4. Despite the morphological differences in the diffusive barriers, the film shows good protective capacity. (Muñoz-Portero et al., 2006) indicate that the morphology of the corrosion products depend on the Br^- concentration in the solution. According to their results, the diffusive barrier developed in the conditions of this project should show an amorphous and gelatinous morphology associated with a mixture of CuBr y $CuBr_2 \cdot 3Cu(OH)_2$.

The records of current and potential noise, show other system characteristics. At 25°C, during the first period, a greater presence of an oxidizing agent in the interface causes an increase in copper dissolution which accelerates the production of CuBr. This substance accumulates on the electrode surface promoting the formation of a protective coating that inhibits the activity at the interface, due to its permeable nature, a pitting corrosion process takes place (Figure 5).

Under flow conditions at 45°C, as the solution velocity increases, the mass transport by diffusion contributes less to the dissolution process, Table 1. At higher velocities, the E_{corr} develops at nobler conditions due to increased oxygen presence in the interface. The system behavior under these conditions clearly reflects the importance of oxygen and the diffusion phenomenon of this element in the dissolution process of the alloy.

Given the conditions that occur at higher levels of velocity, greater involvement of an activation process of the cathodic fraction would be expected. A Tafelian behavior does not occur in these conditions. On the other hand, the behavior at higher levels is very similar giving the impression of having reached the same level at the stationary state.

According to the records of the noise signal in current and potential (Figure 6), at 680 and 884 rpm the potential noise signal reaches the stationary state almost from the start of the test, showing no trend in both levels. Despite the difference in potential, ≈ 12 mV, the current noise signal at both levels is practically the same. This suggests that under these conditions the system is in a passive state. As mentioned above, the increase in the electrode

velocity suggests a greater dissolution of copper, leading to greater nickel presence on the electrode surface.
The system E_{corr}, Table 1, under these conditions is very close to the Flade potential, equation 17, with a difference of 37.4 mV at 680 rpm and only 25.6 mV at 884 rpm, which is why it is not unreasonable to suppose that under these conditions a passive process by chemisorption is developed.

4. Appendices

4.1 Appendix A

Calculation of Gibbs free energy
Calculation of heat capacity C_p^o (Heng & Johnston, 1952; Dean, 1989) in function of absolute temperature for pure substances CuBr.

$$C_p^o = 49.898 + 0.0169\ T - 1.769 \times 10^{-6}\ T^{-2} \tag{A1}$$

The method for determination the heat capacity C_p^o of ionic species, Br^- is that proposed by (Criss & Cobble, 1964; Taylor, 1978) for T< 200ºC, values of absolute entropy and the value of the parameters: a = -0.37 and b = 0.0055 (Roberge, 2000).

$$C_p^o = \left[\left(4.186\ a + b\ S_{(298\ K)}^o\right)\left(T_2 - 298.16\right)\right] \Big/ \ln\left(T_2/298.16\right) \tag{A2}$$

Calculation of Gibbs free energy in the temperature range

$$G_{(T)}^o = G_{(298\ K)}^o + \left(C_p^o - S_{(298\ K)}^o\right)\left(T_2 - 298.16\right) - C_p^o\ T_2\ \ln\left(\frac{T_2}{298.16}\right) \tag{A3}$$

Calculation of equilibrium potential E^o for the reaction of copper dissolution

$$Cu + Br^- \Leftrightarrow CuBr + 1\ e^- \tag{A4}$$

$$E_{(T)}^o = \frac{-\Delta G^o}{n\ F}\ ;\ \left(V_{(SHE)}\right) \tag{A5}$$

Calculation of the potential of equation A4

$$E_{(T)} = E_{(T)}^o + 0.0591 \log\left(\frac{1}{Br^-}\right) \tag{A6}$$

Where Br^- is the activity of bromide ion

4.2 Appendix B

Physicochemical properties of the LiBr-H_2O pair (Torres Merino, 1997)
Calculation of the LiBr solution density based on the density of water, d `Alefeld equation

$$\rho_{(X_{sol},T_{sol})} = \frac{\rho_{H_2O(T_{sol})}}{2}\left[\exp\left(0.012 X_{sol}\right) + \exp\left(\left(0.842 + 1.6414 \times 10^{-3}\ T_{sol}\right)\left(\frac{X_{sol}}{100}\right)^2\right)\right] \tag{B1}$$

Where:

$\rho_{H_2O}(T_{sol})$, water density at the solution temperature, kg m^{-3}; $\rho_{(X_{sol}, T_{sol})}$, solution density, kg m^{-3}; X_{sol}, (mass% LiBr)
Domain range: 40% ≤ X_{sol} ≤ 75%; 0°C ≤ T_{sol} ≤ 190 °C
Calculation of dynamic viscosity μ d'Alefeld equation

$$\mu = \exp\left[A_1 + \frac{A_2}{T_{sol}} + A_3 \cdot \ln T_{sol} \right] \quad \text{(B2)}$$

Where:
A_1 = - 494.122 + 16.3967 X_{sol} – 0.14511 $(X_{sol})^2$; A_2 = 28606.4 – 934.568 X_{sol} + 8.52755 $(X_{sol})^2$; A_3 = 70.3848 – 2.35014 X_{sol} + 0.0207809 $(X_{sol})^2$; μ = dynamic viscosity, cp; T_{sol} = Temperature solution, K; X_{sol} = mass %, LiBr
Domain: 45% ≤ X_{sol} ≤ 65% ; 30°C ≤ T_{sol} ≤ 210°C

4.3 Appendix C

Calculation of the activity of LiBr-H_2O solution.
The model for calculating the activity of strong electrolytes in aqueous solution is proposed by (Meissner et al., 1972; Meissner & Tester, 1972). The calculation of the activity coefficient for a strong electrolyte solution at 25°C is as follows

$$\Gamma^o = \left[1 + B\left(1 + 0.1\, I\right)^q - B \right] \Gamma^* \quad \text{(C1)}$$

With:

$$B = 0.75 - 0.065\, q \quad \text{(C2)}$$

$$\log \Gamma^* = \left(-5107 \sqrt{I}\right) \Big/ \left(1 + C \sqrt{I}\right) \quad \text{(C3)}$$

$$C = 1 + 0.055\, q \exp\left(-0.023\, I^3\right) \quad \text{(C4)}$$

where Γ^o is the reduced activity coefficient of the pure solution at 25°C, q is the Meissner parameter (q = 7.27 for LiBr) I is the ionic strength of electrolyte

$$I = \frac{\sum m_i Z_i^2}{2} = m_{LiBr} \quad \text{(C5)}$$

Z is the number of charges on the cation or anion (Z = 1 for LiBr)
The average ionic activity coefficient for LiBr-H_2O solution

$$\gamma_{\pm} = \left(\Gamma^o\right)^{Z_+ Z_-} = \Gamma^o \quad \text{(C6)}$$

Finally, the activity of the LiBr solution is given by the expression

$$a_{(LiBr)} = \frac{m_{LiBr}}{m^o} \gamma_{\pm} \quad \text{(C7)}$$

Where m^o is the standard solution molality (1 mol LiBr/kg H_2O)

The calculation of the Kusik-Meissner parameter (Kusik & Meissner, 1978) for temperature t in ^{o}C is given by the following equation

$$q_t = \left(a\, q_{(25)} + b^*\right)(t - 25) + q_{(25)} \quad \text{(C8)}$$

Where:
$a = -0.005$ and $b^* = 0.0085$

5. Conclusions

Both the 90% Cu-10% Ni alloy and copper are dissolved, in the Tafel region, by a mechanism consisting of two steps that occur simultaneously. However, the kinetics of copper dissolution results in significant changes in the dissolution process of the alloy.
Corrosion potential in more active regions and smaller corrosion rates due to the presence of nickel in the alloy, generate significant differences between these metals.
Due to the fact that the 90% Cu-10% Ni-X% LiBr system always polarized in comparison to the nickel equilibrium potential, and only sometimes compared to the copper equilibrium potential, the anodic reaction can not be considered reversible, and according to the dissolution mechanism, is under activation control.
According to the proposed equivalent circuit, the dissolution process of the alloy is in fact under a mixed kinetic control, by activation and diffusion. However, the mass transport resistance under all experimental conditions is higher than that observed for charge transfer. On the other hand, as both elements are part of a series, the one representing the mass transport process is the one that shows a greater resistance to current flow. Thus, the diffusion phenomenon must be the process that controls the dissolution of the alloy.
For the dissolution process to be maintained, the reacting species must match at the interface in an electrochemical process. In this sense the complex ion is generated at the interface of the film (equation 13) and spreads to the bulk of the solution. Therefore, oxygen is responsible for the diffusion phenomenon, and does not always follow the Levich relationship.

6. Acknowledgment

The authors acknowledge Consejo Nacional de Ciencia y Tecnología (CONACyT) for financial assistance for the realization of this work. Berenice Adame for her assistance in the translation of this document.

7. References

Bard A. J. & Faulkner L. R. (1980). *Electrochemical Methods Fundamentals and Applications*, ISBN 0-471-04372-9 John Wiley & Sons, Inc., Published in the United States of America simultaneously in Canada

Barsoukov E. & Macdonald J. Ross. (2005). *Impedance Spectroscopy Theory, Experiment, and Applicatons*, second edition. Wiley-Interscience. A John Wiley & Sons, Inc., Publication. 0-471-64749-7, Hoboken, New Jersey. Published simultaneously in Canada.

Beccaria A. M. & Crousier J. (1989). Dealloying of Cu-Ni alloys in natural sea water. *Br. Corros. J.*, Vol. 24, No. 1, (march 1988), pp. 49-52

Bockris J. O`M, Reddy A. K. N. & Gamboa-Aldeco M. (2000). *Modern Electrochemistry Fundamentals of Electrodics*, *Vol. 2A (second edition),* Kluwer Academic/Plenum

Publishers, New York, 0-306-46166-8 (Hardbound), 0-306-46167-6 (paperbound), Printed in the United States of America

Brossard L. (1984). Potentiodynamic Investigation of Copper in LiCl Solutions. *Corrosion,* Vol. 40, No. 8, (august 1984), pp. 420-425

Brossard L. (1984). Potentiodynamic Investigation of Copper in the Presence of Bromide Ions. *J. Electrochem. Soc*., Vol. 131, No. 8, (1984), pp. 1847-1849

Brossard R. L. & Raynaud G. M. (1985). Influence of Temperature on copper bromide formation and dissolution. *Can. J. Chem*., Vol. 63, (april 1984), pp. 720-724

Cooper R. S. & Bartlett J. H. (1958). Convection and Film Instability, Copper anodes in Hydrochloric Acid. *Journal of the Electrochemical Society*, Vol. 105, No. 5, (march 1958), pp. 109-116

Copper-Nickel Alloys in Marine Environments, available from, http:/www.copper.org/applications/cuni/visual_overview/full-text.htm

Criss C. M. & Cobble J. W. (1964). The Thermodynamic Properties of High Temperature Aqueous Solutions. IV. Entropies of the ions up to 200ºC and the Correspondence Principle. *J. Am. Chem Soc.,* Vol. 86, (december 1964), pp. 5385-5401

Crundwell F. K. (1991). The Anodic Dissolution of 90% Copper-10% Nickel alloy in Hydrochloric Acid Solution. *Electrochimica Acta*, Vol. 36, No. 14, (february 1991), pp. 2135-2141

Dean John A. (1989). Manual de Química Lange, Decimotercera Edición McGraw-Hill, 13ª edición, 968-422-087-1 (obra completa) Tomo IV, paginas, 9-20, 9-106, 9-107, 9-118 Impreso en México

Deslouis C., Tribollet B., Mengoli G. & Musiani M. M. (1988). Electrochemical behaviour of copper in neutral aereated chloride solution. I Steady-State investigation. *Journal of Applied Electrochemistry*, Vol. 18, (october 1987), pp. 374-383

Deslouis C., Tribollet B., Mengoli G. & Musiani M. M. (1988). Electrochemical behaviour of copper in neutral aereated chloride solution. II Impedance investigation. *Journal of Applied Electrochemistry*, Vol. 18, (october 1987), pp. 384-393

Deslouis C., Mattos O. R., Musiani M. M. & Tribollet B. (1993). Comments on Mechanism of copper electrodissolution in chloride media. *Electrochimica Acta*, Vol. 38, No. 18, (july 1993), pp. 2781-2783

Dhar H. P., White R. E., Darby R., Cornwell L. R., Griffin R. B. & Burnell G. (1985). Corrosion Behavior of 70Cu-30Ni Alloy in 0.5 NaCl and in Synthetic Seawater. *Corrosion*, Vol. 41, pp. 193-196

Flitt H. J. & Schweinsberg D. P. (2005). A Guide to Polarisation curve interpretation: deconstruction of experimental curves typical of the $Fe/H_2O/H^+/O_2$ corrosion system. *Corros. Sci*., 47, (february 2005), pp. 2125-2156

Fontana M. G. & Greene N. D. (1978). *Corrosion Engineering (second edition)* McGraw-Hill Book Company, 0-07-021461-1, Printed in the United States of America

Hack H. P. & Pickering H. W. (1991). AC Impedance Study of Cu and Cu-Ni Alloys in Aerated Salt Water. I. Pd Coating and Corrosion Product Stripping. *J. Electrochem*. Soc., Vol. 138, No. 3, (March 1991), pp. 690 – 695

Hassibi A., Navid R., Dutton R. W. & Lee T. H. (2004). Comprehensive study of noise processes in electrode electrolyte interfaces. *Journal of Applied Physics,* Vol. 96, No. 2, (April 2004), pp. 1074 – 1082

Heng J. & Johnston H. L. (1952). Low Temperature Heat Capacity of Inorganic Solids XII. Heat Capacity and Thermodynamic Properties of Cuprous Bromide from 16 to 300 K. *The Journal of the American Chemical Society*, Vol. 74, (october 1952), pp. 4771-472

Itzhak D. & Greenberg T. (1999). Galvanic Corrosion of a Copper Alloy in Lithium Bromide Heavy Brine Environments. *Corrosion,* Vol. 55, No. 8, (august 1999), pp. 795-799

Kato C., Ateya B. G., Castle J. E. & Pickering H. W. (1980). On the Mechanism of Corrosion of Cu-9.4Ni-1.7Fe Alloy in air Saturated Aqueous NaCl Solution. I Kinetic Investigations. *J. Electrochem. Soc.*, Vol. 127, No. 9, (september 1980), pp. 1890-1896

Kato C., Castle J. E., Ateya B. G. & Pickering H. W. (1980). On the Mechanism of Corrosion of Cu-9.4Ni-1.7Fe Alloy in air Saturated Aqueous NaCl Solution. II Composition of the Protective Surface Layer. *J. Electrochem. Soc.*, Vol. 127, No. 9, (september 1980), pp. 1897-1903

Kato C. & Pickering H. W. (1984). A Rotating Disk Study of the Corrosion Behavior of Cu-9.4Ni-1.7Fe Alloy in Air-Saturated Aqueous NaCl Solution, *J. Electrochem. Soc.*, Vol. 131, No. 6, (june 1984), pp. 1219-1224

Kear G., Barker B. D. & Walsh F. C. (2004). Electrochemical corrosion of unalloyed copper in chloride media – a critical review. *Corrosion Science*, Vol. 46, (december 2002), pp. 109-135

Kear G., Barker B. D., Stokes K. & Walsh F. C. (2004). Electrochemical corrosion behaviour of 90-10Cu-Ni alloy in chloride media – based electrolytes. *Journal of Applied Electrochemistry*, Vol. 34, No. 55, (january 2004), pp. 659-669

Kear G., Barker B. D., Stokes K. R. & Walsh F. C. (2007). Electrochemistry of non-aged 90-10 copper-nickel alloy (UNS C70610) as a function of fluid flow Part 1: Cathodic and anodic characteristics. *Electrochimica Acta*, Vol. 52, (july 2006), pp. 1889-1898

Kusik C. L. & Meissner H. P. (1978). Electrolyte Activity Coefficients in Inorganic Processing. Fundamentals Aspects of Hydrometallurgical Processes, *AIChE* Symposium Series, Vol. 74, No.173, (1978), pp. 14-20

Kutz M. (2002). *Handbook of Materials Selection*, John Wiley & Sons, Inc., New York United States of America

Lee H. P. & Nobe K. (1984). Rotating Ring-Electrode Studies of Cu-Ni Alloy Electrodissolution in Acidic Chloride Solution, A Commercial Cu-Ni (90/10) Alloy. *J. Electrochem. Soc.*, Vol. 131, No. 6, (june 1984), pp. 1236-1243

Mansfeld F. & Uhlig H. H. (1970). Effect of Electron Donor and Acceptor Elements an Passivity of Copper-Nickel Alloys. *J. Electrochem. Soc.*, Vol. 117, No. 4, (april 1970), pp. 427-432

Mansfeld F. (1973). Simultaneous Determination of Instantaneous Corrosion Rates and Tafel Slopes from Polarization Resistance Measurements. *J. Electrochemical Soc.*: ELECTROCHEMICAL SCIENCE AND TECHNOLOGY. Vol. 120, (april 1973), pp. 515-518

Mansfeld F. (1973). Tafel Slopes and Corrosion Rates from Polarization Resistance Measurements, *Corrosion*, Vol. 29, No. 10, (october 1973), pp. 397-402

Martínez-Meza E. (2011). Corrosión e Inhibición Sobre Acero, Cobre y Aleaciones en Solución Refrigerante de Bromuro de Litio, Empleada en Bombas de Calor. *Ph. D Tesis*. Universidad Nacional Autónoma de México, México D.F.

Meissner H. P. & Tester J. W. (1972). Activity Coefficients of Strong Electrolytes in Aqueous Solutions. *Ind. Eng. Chem. Process Des. Develop*., Vol. 11, No. 1, pp. 128-133

Meissner H. P., Kusik C. L. & Tester J. W. (1972). Activity Coefficients of Strong Electrolytes in Aqueous Solutions-Effect of Temperature. *AIChE Journal*, Vol. 18, No. 3, (may 1972), pp. 661-662

Milosev I. & Metikos H. M. (1997). The behaviour of Cu-$_x$Ni (x = 10 to 40 %) alloys in alkaline solutions containing chloride ions. *Electrochimica Acta*, Vol. 42, No. 10, (september 1996), pp. 1537-1548

Montañés M. T., Pérez-Herranz V., García-Antón J. & Guiñon J. L. (2006). Evolution with Exposure Time of Copper Corrosion in a Concentrated Lithium Bromide Solution Characterization of Corrosion Products by Energy-Dispersive X-Ray Analysis and X-Ray Diffraction. *Corrosion*, Vol. 62, No. 1, (january 2006), pp. 64-73

Muñoz-Portero M. J., García-Antón J., Guiñon J. L. & Pérez-Herranz V. (2006). Corrosion of Copper in Aqueous Lithium Bromide Concentrated Solutions by Immersion Testing. *Corrosion,* Vol. 62, No. 11, (november 2006), pp. 1018-1027

Muñoz-Portero M. J., García-Antón J., Guiñon J. L. & Pérez-Herranz V. (2005). Anodic Polarization Behavior of Copper in Concentrated Aqueous Lithium Bromide Solutions and Comparison with Pourbaix Diagrams. *Corrosion*, Vol. 61, No. 5, (may 2005), pp. 464-472

Muñoz-Portero M. J., García-Antón J., Guiñòn J. L. & Pérez-Herranz V. (2007). Pourbaix Diagrams for Níckel in Concentrated Aqueous Lithium Bromide Solutions at 25 ^{o}C. *Corrosion*, Vol. 63, No. 7, (july 2007), pp. 625-634

Muñoz-Portero M. J., García-Antón J., Guiñòn J. L. & Pérez-Herranz V. (2004). Pourbaix Diagrams for Copper in Aqueous Lithium Bromide Concentrated Solutions. *Corrosion*, Vol. 60, No. 8, (august 2004), pp. 749-756

Othmer K. (2004). *Encyclopedia of Chemical Technology 5th edition*, John Wiley & Sons, Inc., New York, NY United States of America, pp. 679

Pérez-Herranz V., Montañés M. T., García-Antón J. & Guiñon J. L. (2001). Effect of Fluid Velocity and Exposure Time on Copper Corrosion in a Concentrated Lithium Bromide Solution. *Corrosion*, Vol. 57, No. 10, (october 2001), pp. 835-842

Roberge P. R. (2000). *Handbook of Corrosion Engineering*. McGraw Hill. 0-07-076516-2 Appendix D, Electrochemistry Basics, pp. 1011-1059. United States of America.

Stern M. & Geary A. L. (1957). Electrochemical Polarization. I. A Theoretical Analysis of the Shape of Polarization Curves, *J. Electrochem. Soc.,* Vol. 104, No. 1, (january 1957), pp. 56-63

Tan Y. J., Bayley S. & Kinsella B. (1996). The Monitoring of the Formation and Destruction of Corrosion Inhibitor Films Using Electrochemical Noise Analysis (ENA). *Corrosion Science*, Vol. 38, No. 10, (Fefruary 1996), pp. 1681 – 1695

Taylor D. F. (1978). Thermodynamic Properties of Metal-Water Systems at Elevated Temperatures. *J. Electrochem. Soc.*, Solid State Science and Technology, Vol. 125, No. 5, (may 1978), pp. 808-812

Torres Merino J. (1997). Ècole Nationale Superieure des Industries Chimiques Laboratoire des Sciences du Genie Chimique, Thèse. Prèsentee a. L'Institut Nacional Polytechnique de Lorraine pour l'obtention du Titre de Docteur de l'Inpl Spècialite Genie des Procedes par Jesús Torres Merino. Ingenier en Genie Chimique UNAM. Sujet: "Contacteurs Gaz-Liquide pour Pompes a Chaleur a Absortion Multi-Ètages", Fèvrier 1997

Uhlig H. H. & Revie R. W. (1985). *Corrosion and Corrosion Control, An Introduction to Corrosion Science and Engineering, Third Edition*. John Wily & Sons. A Wiley Interscience Publication, 0-471-07818-2, United States of America, Published simultaneously in Canada.

Valero-Gómez A., Igual-Muñoz A. & García-Antón J. (2006). Corrosion and Galvanic Behavior of Copper and Copper-Brazed Joints in Heavy Brine Lithium Bromide Solutions. *Corrosion*, Vol. 62, No. 12, (december 2006), pp. 1117-1131

Weast R. C. (1984). *Handbook of Chemistry and Physics* (65th ed). CRC Press, Inc. 0-8493-0465-2. Boca Raton FL. United States of America

Wood R. J. K., Hutton S. P. & Schiffrin D. J. (1990). Mass Transfer Effects of Non-Cavitating Seawater on the Corrosion of Cu and 70Cu-30Ni. *Corrosion Science*, Vol. 30, No. 12, (december 1989), pp. 1177-1201

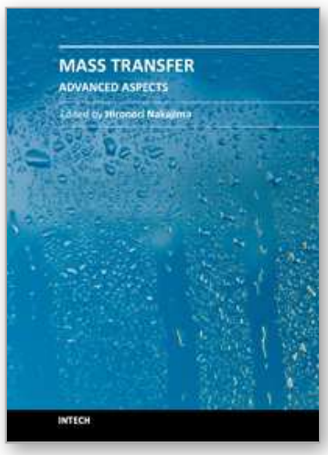

Mass Transfer - Advanced Aspects

Edited by Dr. Hironori Nakajima

ISBN 978-953-307-636-2
Hard cover, 824 pages
Publisher InTech
Published online 07, July, 2011
Published in print edition July, 2011

Our knowledge of mass transfer processes has been extended and applied to various fields of science and engineering including industrial and manufacturing processes in recent years. Since mass transfer is a primordial phenomenon, it plays a key role in the scientific researches and fields of mechanical, energy, environmental, materials, bio, and chemical engineering. In this book, energetic authors provide present advances in scientific findings and technologies, and develop new theoretical models concerning mass transfer. This book brings valuable references for researchers and engineers working in the variety of mass transfer sciences and related fields. Since the constitutive topics cover the advances in broad research areas, the topics will be mutually stimulus and informative to the researchers and engineers in different areas.

How to reference

In order to correctly reference this scholarly work, feel free to copy and paste the following:

Martînez-Meza E., Uruchurtu Chavarîn J. and Genescá Llongueras J. (2011). Mass Transfer in the Electro-Dissolution of 90% Copper-10% Nickel Alloy in a Solution of Lithium Bromide, Mass Transfer - Advanced Aspects, Dr. Hironori Nakajima (Ed.), ISBN: 978-953-307-636-2, InTech, Available from: http://www.intechopen.com/books/mass-transfer-advanced-aspects/mass-transfer-in-the-electro-dissolution-of-90-copper-10-nickel-alloy-in-a-solution-of-lithium-bromi

INTECH
open science | open minds

InTech Europe
University Campus STeP Ri
Slavka Krautzeka 83/A
51000 Rijeka, Croatia
Phone: +385 (51) 770 447
Fax: +385 (51) 686 166
www.intechopen.com

InTech China
Unit 405, Office Block, Hotel Equatorial Shanghai
No.65, Yan An Road (West), Shanghai, 200040, China
中国上海市延安西路65号上海国际贵都大饭店办公楼405单元
Phone: +86-21-62489820
Fax: +86-21-62489821

IntechOpen